*Energy Fuels* **2010,** *24,* 1051–1062 · DOI:10.1021/ef900599v
Published on Web 01/27/2010

energy&fuels
article

# Effect of Chemical Composition on Asphaltenes Aggregation

Emmanuelle Durand,[†,‡] Martin Clemancey,[‡] Jean-Marc Lancelin,[‡] Jan Verstraete,[†] Didier Espinat,[†] and Anne-Agathe Quoineaud*[,†]

[†]*Institut Français du Pétrole (IFP), BP 3, 69360 Solaize, France and* [‡]*Université de Lyon, Université Claude Bernard−Lyon 1, Sciences Analytiques, CNRS UMR 5180, Domaine scientifique de la Doua, ESCPE-Lyon, 69622 Villeurbanne, France*

*Received June 12, 2009. Revised Manuscript Received December 14, 2009*

$^1$H DOSY NMR experiments were used to investigate the macrostructure of the asphaltenes of Maya, Athabasca, and Buzurgan feedstocks in toluene-$d_8$ at 20 °C. The influence of the concentration of asphaltenes on their diffusion coefficients is presented for the three asphaltenes. A separation between two classes of aggregates—one diffusing quickly and one diffusing more slowly—was observed at an onset concentration that is dependent upon the origin of the sample. This illustrates that the chemical interactions (and, hence, the chemical structures) are different for the three asphaltenes. Because asphaltenes are a continuum of both archipelago and continental asphaltenes, the interactions in the solutions differ, depending on the repartition between archipelago- and continental-type asphaltenes in the feed. Maya and Buzurgan asphaltenes show similar diffusion properties in the dilute regime, while Athabasca asphaltenes diffuse more slowly. Results obtained from DOSY experiments data seem to indicate that Buzurgan asphaltenes show a more continental character than the two other asphaltenes, while Athabasca asphaltenes seem to contain more archipelago asphaltenes. $^1$H and $^{13}$C NMR experiments were also performed to determine the average structural parameters of asphaltenes. Average sizes and molecular weights were determined from the $^1$H-DOSY NMR diffusion coefficients and compared to size exclusion chromatography (SEC) data.

## 1. Introduction

Heavy and extra-heavy crude oils represent important energy reserves and, therefore, are becoming increasingly more important, in terms of exploration and upgrading. Heavy oil fractions can be upgraded through various processes, such as visbreaking and hydroprocessing. The main problem to address during upgrading is the presence of asphaltenes. Asphaltenes consist of high-molecular-weight molecules with a pronounced aromatic character that are surrounded by aliphatic chains.[1] They also contain some heteroatoms (nitrogen, sulfur, oxygen) and metals in trace amounts (nickel and vanadium), whose proportions are dependent upon the origin of the sample.[2−4] Vanadium and nickel are the most abundant metals and are often present as chelated porphyrin complexes, which are known to poison the catalysts during hydrotreatment processes.[5] Asphaltenes represent the heaviest and the most polar fraction of the crude oil. They are macromolecules with a self-assembling capacity in nonpolar organic solvents (*n*-heptane or *n*-pentane), as well as in crude oils.[6] They are defined as a solubility class of components: toluene-soluble and insoluble in light *n*-alkane (e.g., *n*-pentane or *n*-heptane).

Over the years, much attention has been given to asphaltenes. They are known to form aggregates that lead to serious problems during oil recovery, transport, and upgrading processes.[7−13] Indeed, they can plug tubings and pipelines, and they also can settle in transportation tankers or storage tanks. Moreover, deposition in distillation columns during refinery operation has also been observed. Furthermore, asphaltenes contribute to catalyst deactivation. As a result, they cause a loss of productivity and an increase of the overall operating cost. Asphaltene aggregates are commonly formed in solvents such as toluene, tetrahydrofuran (THF), and pyridine.[14] Their stability is dependent upon several factors, including temperature, pressure, and also their concentration.[15−17] Asphaltenes form nanoaggregates at very low concentrations.[18] At increasing concentrations, asphaltenes

*Author to whom correspondence should be addressed. Tel.: +33-4-78-02-29-63. Fax: +33-4-78-02-27-45. E-mail: A-Agathe.QUOINEAUD@ifp.fr.

(1) Pfeiffer, J. P.; Saal, R. N. J. *J. Phys. Chem.* **1940**, *44*, 139–149.
(2) Speight, J. G. Asphaltene Constituents. In *The Chemistry and Technology of Petroleum*; CRC Press: Boca Raton, FL, 2007; pp 315−344.
(3) Gawrys, K. L.; Blankenship, G. A.; Kilpatrick, P. K. *Energy Fuels* **2006**, *20*, 705–714.
(4) Spiecker, P. M.; Gawrys, K. L.; Kilpatrick, P. K. *J. Colloid Interface Sci.* **2003**, *267*, 178–193.
(5) Mitra-Kirtley, S.; Mullins, O. C.; Van Elp, J.; George, S. J.; Chen, J.; Cramer, S. P. *J. Am. Chem. Soc.* **1993**, *115*, 252–258.
(6) Pekerar, S.; Lehmann, T.; Mendez, B.; Acevedo, S. *Energy Fuels* **1999**, *13*, 305–308.
(7) Tanaka, R.; Sato, S.; Takanohashi, T.; Hunt, J. E.; Winans, R. E. *Energy Fuels* **2004**, *18*, 1405–1413.
(8) Storm, D. A.; Edwards, J. C.; Decanio, S. J.; Sheu, E. Y. *Energy Fuels* **1994**, *8*, 561–566.
(9) Merdrignac, I.; Espinat, D. *Oil Gas Sci. Technol.* **2007**, *62*, 7–32.
(10) Ancheyta, J.; Centeno, G.; Trejo, F.; Marroquin, G. *Energy Fuels* **2003**, *17*, 1233–1238.
(11) Havre, T. E.; Sjöblom, J. *Colloids Surf. A* **2003**, *228*, 131–142.
(12) Zhao, B.; Zhang, X.; Shaw, J. M. *Energy Fuels* **2008**, *22*, 1747–1758.
(13) Yudin, I. K.; Anisimov, M. A. Dynamic Light Scattering Monitoring of Asphaltenes Aggregation in Crude Oils and Hydrocarbons Solutions. In *Asphaltenes, Heavy Oils, and Petroleomics*; Springer: New York, 2007; pp 439−468.
(14) Trejo, F.; Ancheyta, J.; Morgan, T. J.; Herod, A. A.; Kandiyoti, R. *Energy Fuels* **2007**, *21*, 2121–2128.
(15) Espinat, D.; Fenistein, D.; Barre, L.; Frot, D.; Briolant, Y. *Energy Fuels* **2004**, *18*, 1243–1249.
(16) Buenrostro-Gonzalez, E.; Lira-Galeana, C.; Gil-Villegas, A.; Wu, J. Z. *AIChE J.* **2004**, *50*, 2552–2570.
(17) Shaw, J. M.; Zou, X. Phase Behavior of Heavy Oils. In *Asphaltenes, Heavy Oils, and Petroleomics*; Springer: New York, 2007; pp 489−510.

 

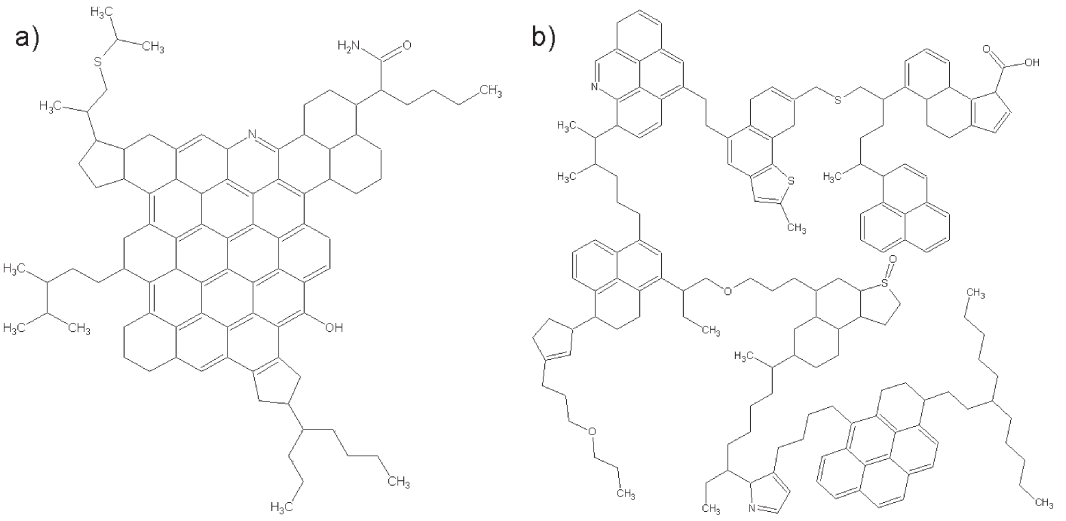


**Figure 1.** Illustrations of (a) the continental model and (b) the archipelago model.

subsequently go from the monomeric entity to nanoaggregates, which can further cluster into larger species[19] or even flocculate. Asphaltenes are known to form nanoaggregates at concentrations lower than 200 mg/L.[7,20−22]

Although asphaltenes have been extensively studied over the last seven decades, their composition and molecular structure still remain an unfolding story, as stated by Strausz et al.[23] Even basic scientific data such as molecular weight, size, shape, and molecular structure are still not yet clearly established and represent big issues in the characterization of asphaltenes. The complexity of the study is due to the nature of asphaltenes themselves: they are composed of polydisperse entities, both in terms of molecular weight and chemical composition. The influence of chemical composition and of the surrounding medium is not well-defined either. Many attempts have been made so far to relate their reactivity to their chemical structure. As a result, it is absolutely necessary to better understand these species so as to be able to develop new catalysts and new conversion processes.

The characterization of asphaltenes is poorly understood, because they are very complex mixtures. Their molecular structure is the least well-defined of the species in the crude oil, because it also is dependent on their origin and the method of recovery. It has been a central enigma of petroleum chemistry.[23] Two different structural model approaches have been proposed for asphaltenes. According to the continental model,[24,25] which is also called the "island model" or the "like your hand model" (see Figure 1a), asphaltenes are shaped as a condensed aromatic molecule. They are composed of one or two polycyclic aromatic hydrocarbons (PAHs)[26,27] per molecules that may be substituted by some alkyl chains. This model supports that the attraction between asphaltene molecules is driven by the interactions between the polyaromatic sheets and is limited by the steric repulsions between the aliphatic chains surrounding the aromatic core.[28]

On the other hand, the "archipelago model" (Figure 1b)[2,23,29−31] represents asphaltenes by means of several small fused-ring systems that are interconnected by alkyl chains and thioether bridges. Even though ring−ring interactions are not favored due to steric considerations, aggregation of asphaltenes of the archipelago type occurs by bridging and hydrogen bonding.[32]

Furthermore, determination of the molecular weight is also a big issue, and the results are still subject to controversy.[25] Many analytical techniques are commonly used to analyze asphaltenes: size exclusion chromatography (SEC),[33] fluorescence depolarization (FD),[34] fluorescence correlation spectroscopy (FCS),[25] mass spectrometry (MS),[35−37] small-angle X-ray scattering (SAXS),[38−40] small-angle neutron scattering (SANS),[31,41,42] calorimetric measurements,[17] vapor pressure osmometry (VPO),[4] and, more recently, scanning electron

(18) Acevedo, S.; Ranaudo, M. A.; Pereira, J. C.; Castillo, J.; Fernandez, A.; Perez, P.; Caetano, M. *Fuel* **1999**, *78*, 997–1003.
(19) Zeng, H.; Song, Y. Q.; Johnson, D. L.; Mullins, O. C. *Energy Fuels* **2009**, *23*, 1201–1208.
(20) Andreatta, G.; Bostrom, N.; Mullins, O. C. *Langmuir* **2005**, *21*, 2728–2736.
(21) Sheu, E.; Long, Y.; Hamza, H. Asphaltene Self-Association and Precipitation in Solvents—AC Conductivity Measurements. In *Asphaltenes, Heavy Oils, and Petroleomics*; Springer: New York, 2007; pp 259−278.
(22) Mostowfi, F.; Indo, K.; Mullins, O. C.; McFarlane, R. *Energy Fuels* **2009**, *23*, 1194–1200.
(23) Strausz, O. P.; Mojelsky, T. W.; Lown, E. M. *Fuel* **1992**, *71*, 1355–1363.
(24) Ruiz-Morales, Y.; Mullins, O. C. *Energy Fuels* **2007**, *21*, 256–265.
(25) Schneider, M. H.; Andrews, A. B.; Mitra-Kirtley, S.; Mullins, O. C. *Energy Fuels* **2007**, *21*, 2875–2882.
(26) Groenzin, H.; Mullins, O. C. *J. Phys. Chem. A* **1999**, *103*, 11237–11245.
(27) Badre, S.; Goncalves, C. C.; Norinaga, K.; Gustavson, G.; Mullins, O. C. *Fuel* **2006**, *85*, 1–11.
(28) Rogel, E. *Langmuir* **2004**, *20*, 1003–1012.
(29) Murgich, J.; Abanero, J. A.; Strausz, O. P. *Energy Fuels* **1999**, *13*, 278–286.
(30) Gray, M. R. *Energy Fuels* **2003**, *17*, 1566–1569.
(31) Gawrys, K. L.; Blankenship, G. A.; Kilpatrick, P. K. *Langmuir* **2006**, *22*, 4487–4497.
(32) Murgich, J. *Mol. Simul.* **2003**, *29*, 451–461.
(33) Merdrignac, I.; Truchy, C.; Robert, E.; Guibard, I.; Kressmann, S. P. *Pet. Sci. Technol.* **2004**, *22*, 1003–1022.
(34) Groenzin, H.; Mullins, O. C. *Energy Fuels* **2000**, *14*, 677–684.
(35) Klein, G. C.; Kim, S.; Rodgers, R. P.; Marshall, A. G.; Yen, A.; Asomaning, S. *Energy Fuels* **2006**, *20*, 1965–1972.
(36) Herod, A. A.; Bartle, K. D.; Kandiyoti, R. *Energy Fuels* **2007**, *21*, 2176–2203.
(37) Qian, K.; Edwards, K. E.; Siskin, M.; Olmstead, W. N.; Mennito, A. S.; Dechert, G. J.; Hoosain, N. E. *Energy Fuels* **2007**, *21*, 1042–1047.
(38) Storm, D. A.; Sheu, E. Y.; Detar, M. M. *Fuel* **1993**, *72*, 977–981.
(39) Barre, L.; Simon, S.; Palermo, T. *Langmuir* **2008**, *24*, 3709–3717.
(40) Sheu, E. Y. *J. Phys.: Condens. Matter* **2006**, *18*, S2485–S2498.
(41) Fenistein, D.; Barre, L.; Broseta, D.; Espinat, D.; Livet, A.; Roux, J. N.; Scarsella, M. *Langmuir* **1998**, *14*, 1013–1020.
(42) Verruto, V. J.; Kilpatrick, P. K. *Energy Fuels* **2007**, *21*, 1217–1225.

microscopy (SEM) and transmission electron microscopy (TEM).[43] However, it is very difficult to establish the physicochemical properties of asphaltenes by conventional techniques,[44] because they have a tendency to form aggregates, depending on their concentration and the solvent that is used. Nuclear magnetic resonance (NMR) is widely used to analyze petroleum samples[45−48] and to determine carbon aromaticity and average carbon parameters.[49−52] Nevertheless, the proton and carbon spectra are crowded and overlapped, because of the presence of numerous aromatic, naphthenic, and aliphatic functions. As a result, a precise chemical structure cannot be established by conventional one-dimensional experiments. Consequently, more-sophisticated NMR sequences are required for the analysis of asphaltenes.

The development of new NMR techniques such as diffusion-ordered two-dimensional (2D) NMR spectroscopy (DOSY),[53] which represents a high-resolution version of the pulsed-field-gradient (PFG) sequences, has allowed researchers to address complex and heterogeneous mixtures, such as biological samples,[54−56] polymers,[57,58] or even intermolecular complexes.[59,60] More recently, it has been used for the analysis of petroleum fractions,[61−63] as well as for measuring protein−ligand interactions.[64] We have recently published[62,65] that DOSY was a suitable tool to analyze asphaltenes. This new technique is expected to provide valuable information concerning the physicochemical properties of asphaltenes, because it is both sensitive to molecular weight and structure. In recent work, Lisitza et al.[63] used DOSY NMR techniques to investigate the molecular dynamics of the initial state of asphaltenes aggregation. They studied asphaltenes at various low concentrations ranging from 0.05 to 2.1 g/L in toluene and showed a kink in the diffusion measurements near 0.2 g/L. From the diffusion coefficient taken on concentrations of $<0.2$ g/L ($D = 2.9 \times 10^{-10}$ m$^2$/s, Stokes−Einstein behavior), the authors extracted an average monomer radius of 1.2 nm, assuming a spherical particle.

Structural and dynamic information (molecular size and also aggregation states) of complex mixtures can be extracted from the measurement of self-diffusion. Diffusion measurements are performed by different analytical techniques such as PFG and fluorescence correlation spectroscopy (FCS).[25,66,67] However, SAXS and SANS analyses are often used to evaluate the size and shape of asphaltene aggregates.[3,39,68−70] DOSY presents the huge advantage of giving, in one experiment, both physical and chemical characterization. Some authors[44,67,71] have already used pulsed-field-gradients spin echo (PFGSE) NMR sequences to analyze asphaltenes, but they have neither shown nor used the bidimensional spectrum of the DOSY sequence. The second dimension offers a rich diffusion spectrum, from which data on the complex composition of the mixture can be obtained. In previous work,[62] we showed the first DOSY spectrum of an asphaltenes sample to demonstrate the potential of these type of sequences to gain insight into the physicochemistry of asphaltene aggregates.

In the current work, we want to study the aggregation behavior of asphaltenes of different origin diluted in toluene over a wide range of concentrations. At the same time, this work also aims at exploring whether there is a correlation between structural parameters of asphaltenes and their aggregation behavior. $^1$H DOSY NMR experiments were used to investigate the macrostructure of the (*n*-heptane insoluble) asphaltenes of Maya, Athabasca, and Buzurgan vacuum residues in toluene-$d_8$ at 20 °C. $^1$H DOSY spectra and diffusion profiles are presented. The influence of the asphaltenes concentration on their diffusion coefficient is illustrated for the three asphaltenes. Results demonstrate that intermolecular interactions between the solvent and the solutes are very dependent upon asphaltenes concentration, as well as the origin of the crude oil. Separation between different classes of asphaltene aggregates was observed above a given threshold concentration, which varies with the origin of the sample.

## 2. Experimental Section

**2.1. Extraction of Asphaltenes.** Asphaltene samples were extracted from three different crude oils: Buzurgan (Middle East crude oil), Athabasca (Canadian crude oil), and Maya (Mexican crude oil). Asphaltenes were precipitated from crude oils with an excess of *n*-heptane at 80 °C, according to a standard analytical procedure derived from the NF T60-115 method. Table 1 presents the saturates, aromatics, resins, and asphaltene (SARA) data of the different analyzed feeds. Mass balances were performed to ensure complete solvent removal.

**2.2. Size Exclusion Chromatography (SEC).** SEC was performed on a Waters 150CV+ system using a refractive index detector. The system was controlled using a Millenium

(43) Trejo, F.; Ancheyta, J.; Rana, M. S. *Energy Fuels* **2009**, *23*, 429–439.
(44) Norinaga, K.; Wargardalam, V. J.; Takasugi, S.; Iino, M.; Matsukawa, S. *Energy Fuels* **2001**, *15*, 1317–1318.
(45) Dickinson, E. M. *Fuel* **1980**, *59*, 290–294.
(46) Morgan, T. J.; George, A.; Davis, D. B.; Herod, A. A.; Kandiyoti, R. *Energy Fuels* **2008**, *22*, 1824–1835.
(47) Desando, M. A.; Lahajnar, G.; Ripmeester, J. A.; Ivan, Z. *Fuel* **1999**, *78*, 31–45.
(48) Nielsen, K. E.; Dittmer, J.; Malmendal, A.; Nielsen, N. C. *Energy Fuels* **2008**, *22*, 4070–4076.
(49) Merdrignac, I.; Quoineaud, A. A.; Gauthier, T. *Energy Fuels* **2006**, *20*, 2028–2036.
(50) Avid, B.; Sato, S.; Takanohashi, T.; Saito, I. *Energy Fuels* **2004**, *18*, 1792–1797.
(51) Sheremata, J. M.; Gray, M. R.; Dettman, H. D.; McCaffrey, W. C. *Energy Fuels* **2004**, *18*, 1377–1384.
(52) Hamaguchi, M.; Nishizawa, T. *Fuel* **1992**, *71*, 747–750.
(53) Morris, K. F.; Johnson, C. S. *J. Am. Chem. Soc.* **1992**, *114*, 3139–3141.
(54) Barjat, H.; Morris, G. A.; Smart, S.; Swanson, A. G.; Williams, S. C. R. *J. Magn. Reson., Ser. B* **1995**, *108*, 170–172.
(55) Hinton, D. P.; Johnson, C. S. *J. Phys. Chem.* **1993**, *97*, 9064–9072.
(56) Morris, K. F.; Johnson, C. S. *J. Am. Chem. Soc.* **1993**, *115*, 4291–4299.
(57) Chen, A.; Wu, D.; Johnson, C. S. *J. Am. Chem. Soc.* **1995**, *117*, 7965–7970.
(58) Jerschow, A.; Muller, N. *Macromolecules* **1998**, *31*, 6573–6578.
(59) Ambrus, A.; Friedrich, K.; Somogyi, A. *Anal. Biochem.* **2006**, *352*, 286–295.
(60) Viel, S.; Mannina, L.; Segre, A. *Tetrahedron Lett.* **2002**, *43*, 2515–2519.
(61) Kapur, G. S.; Findeisen, M.; Berger, S. *Fuel* **2000**, *79*, 1347–1351.
(62) Durand, E.; Clemancey, M.; Quoineaud, A. A.; Verstraete, J.; Espinat, D.; Lancelin, J. M. *Energy Fuels* **2008**, *22*, 2604–2610.
(63) Lisitza, N. V.; Freed, D. E.; Sen, P. N.; Song, Y. Q. *Energy Fuels* **2009**, *23*, 1189–1193.
(64) Lucas, L. H.; Larive, C. K. *Concepts Magn. Reson., Part A* **2004**, *20A*, 24–41.
(65) Durand, E.; Clemancey, M.; Lancelin, J. M.; Verstraete, J.; Espinat, D.; Quoineaud, A. A. *J. Phys. Chem. C* **2009**, *113*, 16266–16276.
(66) Andrews, A. B.; Guerra, R. E.; Mullins, O. C.; Sen, P. N. *J. Phys. Chem. A* **2006**, *110*, 8093–8097.
(67) Ostlund, J. A.; Andersen, S. I.; Nyden, M. *Fuel* **2001**, *80*, 1529–1533.
(68) Espinat, D.; Rosenberg, E.; Scarsella, M.; Barre, L.; Fenistein, D.; Broseta, D. Colloidal Structural Evolution from Stable to Flocculated State of Asphaltene Solutions and Heavy Crudes. In *Structures and Dynamics of Asphaltenes*; Plenum Press: New York, 1998; pp 145−202.
(69) Tanaka, R.; Hunt, J. E.; Winans, R. E.; Thiyagarajan, P.; Sato, S.; Takanohashi, T. *Energy Fuels* **2003**, *17*, 127–134.
(70) Gawrys, K. L.; Kilpatrick, P. K. *J. Colloid Interface Sci.* **2005**, *288*, 325–334.
(71) Kawashima, H.; Takanohashi, T.; Iino, M.; Matsukawa, S. *Energy Fuels* **2008**, *22*, 3989–3993.

**Table 1. Detailed Characterization of Buzurgan, Maya, and Athabasca Feedstocks and Asphaltenes**

| property | Value | | |
|---|---|---|---|
| | Buzurgan | Maya | Athabasca |
| | Feedstocks | | |
| Conradson carbon content | 22.0 wt % | 14.8 wt % | 21.0 wt % |
| $d^{15}{}_4$ | 1.037 | 1.025 | 1.044 |
| viscosity at 100 °C | 2670 cSt | 2295 cSt | 1395 cSt |
| SARA analysis | | | |
| saturates | 9.7 wt % | 12.3 wt % | 4.3 wt % |
| aromatics | 37.7 wt % | 38.5 wt % | 27.2 wt % |
| resins | 35.7 wt % | 36.2 wt % | 51.7 wt % |
| asphaltenes | 16.9 wt % | 13.0 wt % | 16.9 wt % |
| | Asphaltenes | | |
| elemental analysis of the asphaltenes | | | |
| carbon | 81.2 wt % | 83.5 wt % | 80.6 wt % |
| hydrogen | 7.2 wt % | 7.2 wt % | 7.7 wt % |
| H/C | 1.07 | 1.04 | 1.15 |
| nitrogen | 1.1 wt % | 1.0 wt % | 1.3 wt % |
| N/C | 0.01 | 0.01 | 0.01 |
| oxygen | 0.9 wt % | 0.9 wt % | 1.4 wt % |
| O/C | 0.008 | 0.008 | 0.013 |
| sulfur | 8.0 wt % | 5.8 wt % | 8.4 wt % |
| S/C | 0.04 | 0.03 | 0.04 |
| total heteroatoms | 10.0 wt % | 7.7 wt % | 11.4 wt % |
| nickel | 251 ppm | 336 ppm | 388 ppm |
| vanadium | 801 ppm | 1492 ppm | 1110 ppm |

chromatography manager. Columns packed with polystyrene–divinylbenzene supports (PS-DVB, Polymer Laboratories) were chosen; the corresponding porosities are 100, 1000, and 10 000 Å, and the column characteristics are as follows: packing particle size, $d_p = 5\ \mu$m; column length, $L = 300$ mm; and internal diameter, 8 mm. Ten monodisperse polystyrene standards with masses ranging from 162 g/mol to 120 000 g/mol were used to perform the molecular weight calibration. The different asphaltenes samples were injected at a concentration of 5 g/L in tetrahydrofuran (THF) with a volume of 50 $\mu$L. The temperature was fixed at 40 °C, and the flow rate was fixed to 0.7 mL/min. The choice of these operating conditions has been described elsewhere.[33]

**2.3. $^{13}$C Nuclear Magnetic Resonance ($^{13}$C NMR).** The structural parameters of the asphaltenes were measured using $^{13}$C NMR experiments performed on an Avance 300 MHz Bruker spectrometer, using a 10-mm BBO 1H/X/D NMR probe at 25 °C. $^{13}$C NMR experiments were performed using a spectral width of 200 ppm, a relaxation delay of 60 s ,and 512 scans. One hundred milligrams (100 mg) of asphaltenes were diluted in 3 mL of $CDCl_3$ to obtain a homogeneous solution. The chemical shifts were referenced using $CDCl_3$ as the solvent. The Attached Proton Test (APT) series was conducted to identify and quantify the proportion of atoms of carbon, as a function of the number of protons in their neighborhood, as described elsewhere.[72,73] Two $^{13}$C NMR experiments, based on the scalar coupling between protons and carbons, were performed to obtain some data on paraffinic, naphthenic, and aromatic carbon atoms. $^{13}$C NMR direct acquisition spectra were performed with a 60° flip angle at a radio frequency pulse of 20 kHz with a DQD acquisition mode. These experiments provided quantification of saturated and unsaturated C atoms. Moreover, spin–echo $\pi/2-\tau-\pi-\tau$ experiments[74] were set to quantify aromatic and aliphatic species separately.

**2.4. $^1$H DOSY NMR Measurements.** The dynamic behavior of asphaltenes was investigated by $^1$H DOSY NMR. Asphaltenes were diluted in perdeuterated toluene (99.8% D) supplied by Eurisotop. A wide range of concentrations (0.01–15 wt %) in toluene-$d_8$ was investigated and added to 5-mm NMR tubes. DOSY NMR experiments were performed on a Unity-Varian Model 600 spectrometer operating at a $^1$H frequency of 600 MHz equipped with a 5-mm $^1$H-X reverse $z$-axis gradient probe capable of generating 60 G/cm field strengths.

The Doneshot[75] sequence was used to measure solutes and solvent self-diffusion with an $\alpha$ value of 0.2. This sequence will be detailed in a following paragraph. The gradient pulse strength ($g$) was varied in 50 linear steps from 0 G/cm to 60 G/cm to obtain complete signal attenuation. Gradients were calibrated against the HOD diffusion constant at 25 °C ($D_2O$, 99.9%, $D = 19.0 \times 10^{-10}$ m$^2$/s),[76,77] as recommended by Price.[77] The calibration was confirmed by measuring adenosine triphosphate (ATP), sodium dodecyl sulfate (SDS), and glucose diffusion coefficients mixed in $D_2O$ at 22 °C.[56] These molecules, which are heavier than $n$-heptane or $n$-dodecane (commonly used as references for gradients calibration) will better reflect the behavior of heavy petroleum molecules than the $n$-alkane solvents. In the Doneshot sequence, based on a stimulated echo, the gradient pulse duration ($\delta$) and the diffusion delay ($\Delta$) were kept constant, ranging between 0.8 ms and 5.0 ms for $\delta$ and between 0.10 and 0.60 s for $\Delta$. Spectra were acquired at 20 °C with a 90° pulse duration of 6.38 $\mu$s and a relaxation delay of 30 s.

Published DOSY spectra generally use either monoexponential or multiexponential fittings. One of the main advantages of the fitting method is the utilization of least-squares fitting algorithms, which are straightforward and result in fast processing. However, such processing techniques cannot be applied to highly complex mixtures, such as asphaltenes, because they require an assumption for the number of components. The studied polydisperse samples are composed of thousands of unknown constituents. CONTIN[78,79] is able to process the DOSY NMR spectra of polydisperse samples. Nevertheless, this software exhibits insufficient resolution to enable a separation of the different species with similar sizes.[80,81] As a result, NMR data were processed with NMR notebook (from NMR*tec*) with a DOSY module. The Maximum Entropy (MaxEnt) Laplace inversion is implemented in the software.[80] It gives access to the entire diffusion spectrum without using any *a priori* estimate for the number of components present in the sample and, therefore, is well-adapted to polydisperse mixtures. Its goal is to build the inverse Laplace transform using the MaxEnt process. According to the authors, this software provides a high-quality spectrum that ensures the resolution, accuracy, and reliability of the results.[80]

## 3. Theoretical Basis

**3.1. DOSY NMR Theory.** Diffusion ordered spectroscopy (DOSY)[53,81] is a method that was devised by Morris and Johnson.[53] It is a two-dimensional version of the pulsed-field-gradient spin–echo nuclear magnetic resonance (PFGSE NMR) sequence of Stejskal and Tanner,[82] which, itself, was based on the nuclear spin–echo concept of Hahn[74]

(72) Patt, S. L.; Shoolery, J. N. *J. Magn. Reson.* (*1969–1992*) **1982**, *46*, 535–539.
(73) Jakobsen, H. J.; Sorensen, O. W.; Brey, W. S.; Kanyha, P. *J. Magn. Reson.* (*1969–1992*) **1982**, *48*, 328–335.
(74) Hahn, E. L. *Phys. Rev.* **1950**, *80*, 580.
(75) Pelta, M. D.; Morris, G. A.; Stchedroff, M. J.; Hammond, S. J. *Magn. Reson. Chem.* **2002**, *40*, S147–S152.
(76) Antalek, B. *Concepts Magn. Reson.* **2002**, *14*, 225–258.
(77) Price, W. S. *Concepts Magn. Reson.* **1998**, *10*, 197–237.
(78) Provencher, S. W. *Comput. Phys. Commun.* **1982**, *27*, 213–227.
(79) Provencher, S. W. *Comput. Phys. Commun.* **1982**, *27*, 229–242.
(80) Delsuc, M. A.; Malliavin, T. E. *Anal. Chem.* **1998**, *70*, 2146–2148.
(81) Johnson, C. S. *Prog. Nucl. Magn. Reson. Spectrosc.* **1999**, *34*, 203–256.
(82) Stejskal, E. O.; Tanner, J. E. *J. Chem. Phys.* **1965**, *42*, 288–292.

and Carr and Purcell.[83] DOSY NMR experiments allow for resolution and identification of the mixture constituents. It aims at measuring the mobility of each component present in a mixture. Diffusion coefficients are sensitive to size (and, thus, to molecular weight), shape, and aggregation status. The spectrum obtained from such experiment is a bidimensional spectrum in which the first dimension ($x$-axis) is a conventional NMR spectrum (chemical shift), while the diffusion coefficients are presented along the $y$-axis. One of the sequences available for Varian Inova spectrometers is the Doneshot sequence.[75] Based on a PFGSE sequence, it is described by its authors as being a powerful technique for the analysis of mixtures. The Doneshot sequence presents several advantages, compared to the bipolar pulse pair stimulated echo (BPPSTE), from which it was derived. First of all, diffusion measurements can be performed in just one shot and with only one transient per gradient strength without any phase cycling, which enables a relatively short time of analysis. The sequence is composed of extra balancing gradient pulses, in addition to asymmetric bipolar field gradient pulse pairs, to select a unique coherence transfer pathway and, at the same time, minimize the eddy current effect. Some gradients have been added at the beginning and the end of the diffusion delay to keep the deuterium lock signal focused and to minimize field-frequency lock disturbances. Its intention is to keep the system constant. A thorough description of the sequence is given by Pelta et al.[75] In practice, while increasing gradient strengths, the intensity of the signal is attenuated because of diffusion, according to an exponential function. Thus, the diffusion coefficient ($D$) is related to the signal amplitude ($I$) while applying gradient ($g$) in the $z$-direction and to the signal amplitude at zero gradient ($I_0$) in the same direction through eq 1,[75] which is derived from the Stejskal−Tanner equation:

$$I = I_0 \exp\left\{-D\gamma^2 g^2 \delta^2 \left[\Delta + \frac{\delta(\alpha^2-2)}{6} + \frac{\tau(\alpha^2-1)}{2}\right]\right\} \quad (1)$$

where $\delta$ is the width of the field gradient pulses, $\Delta$ the diffusion delay, $\gamma$ the magnetogyric ratio ($2.675 \times 10^8$ rad $T^{-1}$ $s^{-1}$ for $^1H$), $\alpha$ the imbalance factor, and $\tau$ the time between the midpoints of the individual gradient pulses in one diffusion-encoding period. The translational self-diffusion coefficient ($D$) values of the different compounds of the mixture are extracted from this equation.

**3.2. Molecular Mass and Size of Asphaltenes Extracted from the Diffusion Coefficient ($D$).** The Stokes−Einstein equation is often used to extract the hydrodynamic radius $R_H$ of the solute from its diffusion coefficient $D$:

$$D = \frac{k_B T}{6\pi\eta R_H} \quad (2)$$

where $k_B$ is the Boltzmann's constant, $T$ the absolute temperature, and $\eta$ the solvent viscosity. However, this equation was established for spherical particles that are much larger than the solvent molecules ($R_H > 5R_{solv}$), which is obviously not the case here. Hence, the shape and size of the solute also must be taken into account. Therefore, the modified Stokes−Einstein equation[84] is defined by

$$D = \frac{k_B T}{c(R_{solv}, R_H) f_s(a,b) \pi\eta R_H} \quad (3)$$

First of all, the shape and the size of the solute should be taken into account through $f_s$, which is dependent on the ratio between the minor semiaxis ($b$-axis) and the major ($a$) semiaxis of an ellipsoidal molecule. The expression for $f_s$ varies, depending on whether prolate (cigarlike) or oblate (disklike) ellipsoidal molecules are considered[84,85] and could be find elsewhere.[65]

The difficulty with petroleum samples resides in the number of components, because there are thousands of heavy hydrocarbon species with different shapes. Therefore, an average spherical particle is assumed, and $f_s$ is set equal to 1. The simplification is obviously idealized, but establishing an exact $f_s$ value is impossible, given the complexity of the system. Second, the Stokes−Einstein equation has also been revised to account for the actual difference in size of the solute and solvent molecules. Hence, the modified Stokes−Einstein equation contains a correction factor $c$, which is dependent upon the ratio of the radius of the solvent ($R_{solv}$) to that of the solute $R_H$,[84,86] and is equal to

$$c = \frac{6}{1 + 0.695(R_{solv}/R_H)^{2.234}} \quad (4)$$

Besides the hydrodynamic radius or size of the molecule, one can also go a step further and determine a molecular weight from diffusion measurements. A well-known relationship[58,87] that relates the diffusion coefficient $D$ to the molecular weight $M$ has been established by combining the Flory scaling law ($R_g \propto M^{-\alpha}$, where $R_g$ is the radius of gyration) valid in the dilute regime and the Stokes−Einstein equation (as for a spherical particle $R_g \propto R_H$):

$$D = KM^{-\alpha} \qquad (\alpha > 0) \quad (5)$$

where $K$ is a constant that is dependent upon the nature of the molecule and $\alpha$ a coefficient, termed the shape factor, that is dependent upon the shape of the particle.[88] From a theoretical point of view, the value of $\alpha$ should be 0.33 for a rigid spherical particle, whereas a value of 0.5 for $\alpha$ would reflect either a random coil oligomer in a $\theta$ solvent or a flat disk. In the case of a good solvent, $\alpha$ should be equal to 0.6.[89] For this method, the use of an internal reference provides several benefits. In this work, the solvent was chosen as the internal reference. Diffusion analysis can be performed on both the solvent and the solute in a single experiment. It improves the accuracy without additional experiment time.[90] This relative diffusivity, as it is called by Jones et al.,[91] is defined as the ratio of the diffusion coefficients of the solute and of the solvent:

$$D_{rel} = \frac{D_{solute}}{D_{solvent}} \quad (6)$$

This approach allows the impact of viscosity or temperature variations to be reduced and, hence, is thought to provide more-robust data.

(83) Carr, H. Y.; Purcell, E. M. *Phys. Rev.* **1954**, *94*, 630.
(84) Macchioni, A.; Ciancaleoni, G.; Zuccacia, C.; Zuccacia, D. *Chem. Soc. Rev.* **2008**, *37*, 479–489.
(85) Perrin, F. *J. Phys. Radium* **1936**, *7*, 1–11.
(86) Chen, H. C.; Chen, S. H. *J. Phys. Chem.* **1984**, *88*, 5118–5121.
(87) Hakansson, B.; Nyden, M.; Soderman, O. *Colloid Polym. Sci.* **2000**, *278*, 399–405.
(88) Augé, S.; Schmit, P. O.; Crutchfield, C. A.; Islam, M. T.; Harris, D. J.; Durand, E.; Clemancey, M.; Quoineaud, A. A.; Lancelin, J. M.; Prigent, Y.; Taulelle, F.; Delsuc, M. A. *J. Phys. Chem. B* **2009**, *113*, 1914–1918.
(89) Cosgrove, T.; Griffiths, P. C. *Polymer* **1995**, *36*, 3335–3342.
(90) Crutchfield, C. A.; Harris, D. J. *J. Magn. Reson.* **2007**, *185*, 179–182.
(91) Jones, J. A.; Wilkins, D. K.; Smith, L. J.; Dobson, C. M. *J. Biomol. NMR* **1997**, *10*, 199–203.

To estimate an average molecular weight for the asphaltene samples from $^1$H DOSY NMR data, a polystyrene (PS) calibration curve was established in previous work.[92] A relative diffusivity−molecular mass calibration curve in a double-logarithmic plot was generated from the experimental results. The data obtained for the PS standards fell on a straight line:

$$\frac{D_{\text{solute}}}{D_{\text{solvent}}} = 10^{-0.144 \pm 0.029} \times \left(\frac{M_{\text{solute}}}{M_{\text{solvent}}}\right)^{-0.42 \pm 0.02} \quad (7)$$

where $D$ is the self-diffusion coefficient and $M$ is the molecular weight. In the following sections, molecular weights from DOSY measurements will be given as polystyrene equivalents. Obtaining an $\alpha$ value of 0.33−0.5 is not surprising; this value reflects a soft interpenetrable sphere, as defined by Pyun and Fixman.[93] This equation will be subsequently used as a calibration curve to determine an average molecular weight of the studied asphaltene samples. Similar scaling laws have been recently observed for asphaltenes for other measured parameters:[39] $R_g = 0.43 M_w^{0.45}$ and $[\eta] = 0.049 M_w^{0.41}$. Moreover, assuming a shape factor of 0.42 for asphaltenes is also consistent with some previous work.[94]

## 4. Results and Discussions

**4.1. Average Chemical Composition.** The chemical composition of the different asphaltenes samples were examined to investigate whether there was a relationship with their aggregation behavior. Table 1 compares the elemental analysis of the asphaltenes, depending on their geographical origin. There is no sufficiently clear difference in the elemental composition of the study's asphaltene samples. Even if these data do not exhibit large variations, from the chemical composition point of view, we can notice significant differences according to the classical range of elemental composition of asphaltenes reported by Speight.[2] We can particularly highlight that the H/C ratio ranges from 1.04 for Maya asphaltenes to 1.15 to Athabasca asphaltenes. We know that this ratio is strongly connected to the asphaltene density. The lower the H/C ratio, the higher the density of asphaltenes (and, consequently, the size of the molecules). Note that the Athabasca asphaltenes contain the highest amount of heteroatoms, relative to the others. The data also show that metals (vanadium and nickel) are more concentrated in the Mexican asphaltenes (Maya) than in the other two types of asphaltenes. Consequently, because the content of heteroatoms varies from one origin to another, the chemical behavior is expected to be different.

The average chemical structures of the asphaltenes have been investigated using $^{13}$C NMR, $^1$H NMR, and a series of Attached Proton Test (APT) NMR analyses[72,73] and spin−echoes. The direct $^{13}$C method is used to quantify the different types of carbon present in the sample. It is possible to determine the total amount of aromatic ($C_{aro}$) and aliphatic ($C_{ali}$) carbon species by integration of the 150−100 ppm and 70−0 ppm chemical shift areas, respectively as shown in Figure 2a.

The $^{13}$C APT NMR method based on the scalar coupling between a carbon and a proton was performed to determine the relative percentages of aromatic, naphthenic, and paraffinic carbons. This sequence enables the distinction between carbons close to an even (quaternary carbons and methylene groups) or an odd (methyne and methyl groups) proton number. APT, corresponding to $^1/_2 J_{CH}$ with $J_{CH} = 160$ Hz is characteristic of protonated aromatic carbons. The quantity of unsubstituted carbons CH ($CH_{aro}$) and quaternary carbon ($C_{q,aro}$), either condensed or substituted ($C_{q,aro} = C_{q,sub} + C_{q,cond}$) (see Figure 2b), that are in the aromatic portion is calculated using integration of the 150−100 ppm region of the $^{13}$C spin−echo and $^{13}$C. APT, corresponding to $^1/_2 J_{CH}$ with $J_{CH} = 125$ Hz (which is typical of $sp^3$ carbons) is characteristic of protonated aliphatic carbons. The percentages of $CH_3$, $CH_2$, CH, and quaternary carbon ($C_q$) present in the aliphatic components are measured using integration of the 70−0 ppm region of the $^{13}$C spin−echo and the $^{13}$C APT NMR.

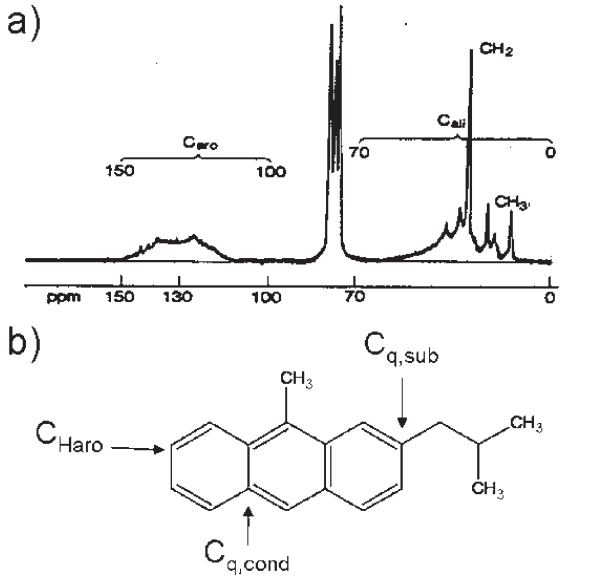


**Figure 2.** (a) $^{13}$C NMR spectrum of asphaltenes. (b) Illustration of different types of aromatic carbons.

Using the amount of total aromatic carbons and the percentages of CH and $C_{q,aro}$, the substitution index can be evaluated. The substitution index ($I_s$) is defined as the ratio between the substituted and the substitutable aromatic carbons:

$$I_s = \frac{C_{q,sub}}{C_{aro} - C_{q,cond}} \quad (8)$$

where $C_{q,cond}$ represents the amount of quaternary condensed aromatic carbons, $C_{q,sub}$ corresponds to the amount of quaternary aromatic carbons that are substituted, and $C_{aro}$ denotes the total amount of aromatic carbons.

It is also possible to calculate the condensation index $I_c$, which represents the average number of condensed aromatic rings. However, two different condensation indices $I_c$ can be calculated. Depending on the structure of the aromatic molecule that is considered (Figure 3), one can calculate the *peri*-condensed index ($I_{cp}$) and the *cata*-condensed index ($I_{cc}$), which are defined as follows:

$$I_{cp} = \frac{1 + 2(C_{q,cond}/C_{aro})}{1 - 3[C_{q,cond}/(2C_{aro})]} \quad (9)$$

$$I_{cc} = \frac{1 + (C_{q,cond}/C_{aro})}{1 - 2(C_{q,cond}/C_{aro})} \quad (10)$$

(92) Durand, E.; Clemancey, M.; Lancelin, J.-M.; Verstraete, J.; Espinat, D.; Quoineaud, A. A. *J. Phys. Chem. C* **2009**, *113* (36), 16266−16276.
(93) Pyun, C. W.; Fixman, M. *J. Chem. Phys.* **1964**, *41*, 937–944.
(94) Nortz, R. L.; Baltus, R. E.; Rahimi, P. *Ind. Eng. Chem. Res.* **1990**, *29*, 1968–1976.

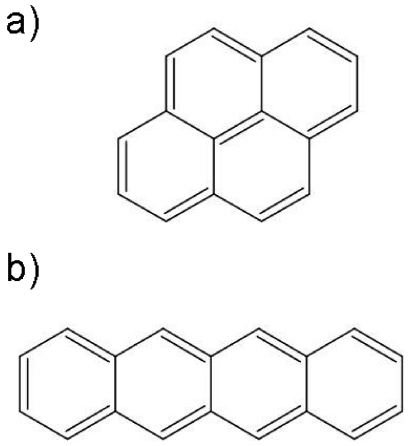


**Figure 3.** Illustration of (a) *peri*-condensed and (b) *cata*-condensed aromatic carbons.

These parameters are used to assess the structure of the studied samples by taking into account the aliphatic, aromatic, alkylated, or polycondensed aromatic characters, the number of aromatic cycles, as well as the length of the alkyl chains. The main NMR data of the asphaltene samples are presented in Table 2.

The aliphatic species can be characterized by means of these $^{13}C$ NMR data. There are either many alkyl chains (which would be consistent with the $C_{q,sub}$ and $I_s$) or the alkyl chains are highly substituted (high $CH_3$ and CH percentage). The first thing to note is that the Athabasca asphaltenes contain more aliphatic carbons ($C_{ali}$) than Maya and Buzurgan asphaltenes. The alkyl chain length (the amount of $CH_2$) is shorter for Buzurgan asphaltenes than for Athabasca asphaltenes. Besides this, Buzurgan asphaltenes contain the highest amount of $CH_3$. These last results suggest that Buzurgan asphaltenes contain few and short alkyl chains. This would be consistent with a more-condensed structure for Buzurgan asphaltenes, whereas Athabasca asphaltenes would be more concentrated in long alkyl chains (the highest $CH_2$ amount). Furthermore, if we focus on the data for the aromatic carbons, we see that most of the aromatic carbons are quaternary (either substituted or condensed). Because the aromatic cores in asphaltenes are composed of a mix of *peri*- and *cata*-condensed structures, the average number of benzene rings in an aromatic core of Buzurgan asphaltenes lies somewhere between 5 (if they are in a pure *peri*-condensed form) and 10 (if they happen to be in a pure *cata*-condensed form) (see Table 2). However, the average number of benzene rings in the aromatic cores of Maya and Athabasca asphaltenes lies between 4 and 5 (Maya) and between 5 and 8 (Athabasca), respectively. These data show that Athabasca and Maya asphaltenes contain smaller aromatic cores than Buzurgan asphaltenes. One should keep in mind that, because the differences reported in Table 2 are not very pronounced, no clear conclusions can be drawn. Indeed, the values are very close and fall within the measurement errors. Hence, the remarks reported are only trends. To conclude, only average chemical parameters can be obtained from $^{13}C$ NMR. There are no significant differences between the various asphaltenes to draw conclusions on their structure and to know whether asphaltenes belong to the archipelago or the continental model. Further information is required to better understand asphaltenes structure and behavior. $^{1}H$ DOSY NMR will be investigated to extract

**Table 2. NMR Data for the Various Asphaltenes**

| | Value | | |
|---|---|---|---|
| type of carbon[a] | Buzurgan | Maya | Athabasca |
| $C_{ali}$ (±2.0%) | 46.8% | 44.7% | 49.8% |
| $CH_3$ (±2.8%) | 12.4% | 8.9% | 10.3% |
| $CH_2$ (±3.0%) | 27.8% | 27.6% | 32.6% |
| CH (±2.8%) | 6.6% | 8.2% | 6.9% |
| $C_q$ (±2.0%) | 0.0% | 0.0% | 0.0% |
| $C_{aro}$ (±2.0%) | 53.2% | 55.3% | 50.2% |
| $CH_{aro}$ (±2.8%) | 11.4% | 13.5% | 10.4% |
| $C_q$ (±2.0%) | 41.8% | 41.8% | 39.8% |
| $C_{q,sub}$ (±2.0%) | 19.0% | 21.3% | 19.4% |
| $C_{q,cond}$ (±2.0%) | 22.8% | 20.5% | 20.4% |
| $I_s$ | 0.63 | 0.60 | 0.65 |
| $I_{cp}$ | 5.2 | 4.0 | 4.6 |
| $I_{cc}$ | 10.1 | 5.3 | 7.8 |
| $C_{ali}/C_{aro}$ | 0.88 | 0.81 | 0.99 |

[a] The value given in parentheses (±$x$%) represents the confidence interval.

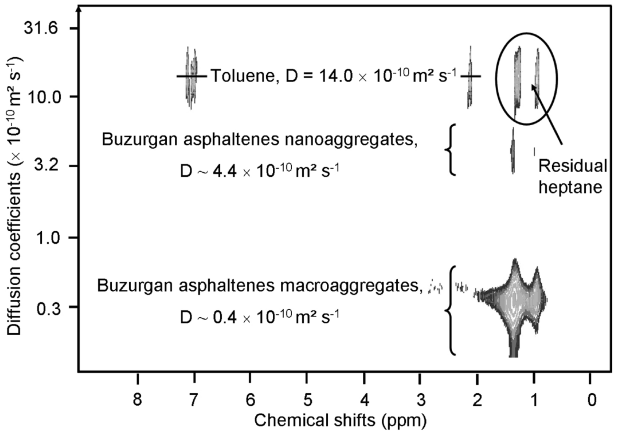


**Figure 4.** $^{1}H$ DOSY NMR spectrum of Buzurgan asphaltenes analyzed at 15 wt % in toluene-$d_8$.

physicochemical parameters of asphaltenes in toluene-$d_8$ over a wide range of concentrations.

**4.2. Evidence of Selective Affinities.** The asphaltenes from three different origins were analyzed in toluene-$d_8$ at different concentrations ranging from 0.01 wt % to 15 wt %. We have already shown that DOSY spectra allow a better resolution in the diffusion dimension,[62] enabling the separation between the solvent and the oil molecules, as shown by Figures 4, 5, and 6, which respectively present the $^{1}H$ DOSY spectra of Buzurgan, Maya, and Athabasca asphaltenes analyzed at 15 wt % in toluene-$d_8$.

Different signals may be extracted from these 2D spectra. First of all, the solvent signals are clearly separated from the asphaltenes signals because the latter diffuse more slowly. This could not be achieved directly in the proton spectrum, because it was too crowded and the signals were overlapped in the chemical shift dimension. It illustrates one of the key advantages of DOSY sequences. Second, although *n*-heptane was supposed to be totally removed from the asphaltenes, the Maya and Buzurgan DOSY spectra obviously show that there are still some residual *n*-heptane molecules. Its presence is not surprising, because asphaltenes are precipitated in an excess of *n*-heptane, according to the NF T60-115 method.

First of all, focusing on the asphaltene signals, the first thing to note is that no aromatic protons were observed. Even if there are few aromatic protons, because of highly

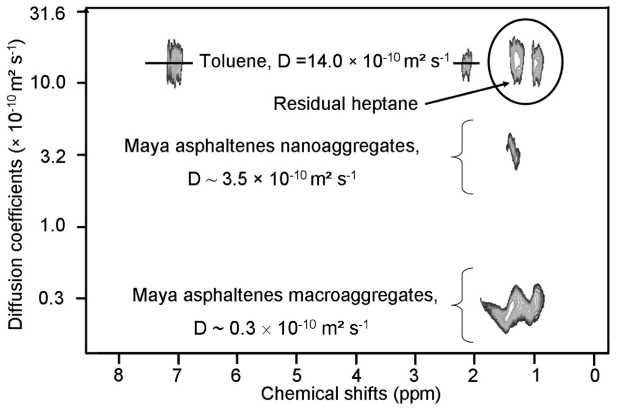


**Figure 5.** $^1$H DOSY NMR spectrum of Maya asphaltenes analyzed at 15 wt % in toluene-$d_8$.

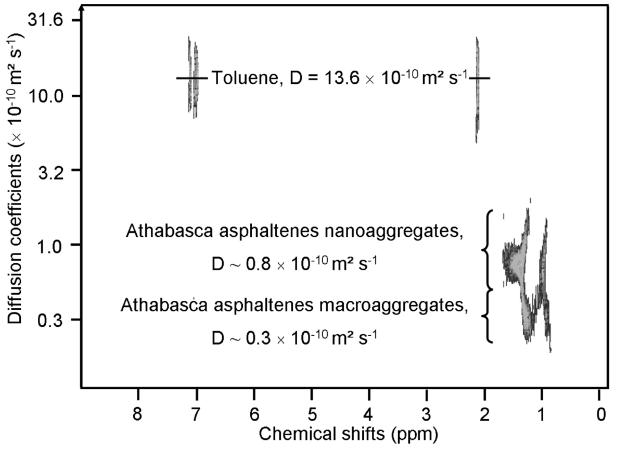


**Figure 6.** $^1$H DOSY NMR spectrum of Athabasca asphaltenes analyzed at 15 wt % in toluene-$d_8$.

substituted aromatic cores, we can guess that they are not observed because of the fast relaxation time (T2) of these types of protons. As already presented,[65] asphaltene peaks are very broad, leading to a reduction of their intensities and especially aromatic signals, which cannot be differentiated from the toluene signals.

Second, focusing on aliphatic signals, two different asphaltene aggregates have been observed and are clearly separated for the Mexican and Buzurgan asphaltenes studied at 15 wt %. The two classes of asphaltene aggregates do not present the same diffusion properties. We can easily imagine that some asphaltene molecules have a more pronounced tendency to aggregate in toluene, leading to a heavier apparent molecular weight and, as a result, a lower mobility. They are called "macroaggregates". However, the second class of aggregates contains asphaltene entities that remain in solution, leading to a lower apparent molecular weight (i.e., a higher diffusion coefficient). This observation reflects huge differences both in terms of molecular weight and hydrodynamic radius between the two types of asphaltene aggregates. Moreover, according to the DOSY spectra, Maya and Buzurgan asphaltenes seem to be richer in macroaggregates, whereas Athabasca asphaltenes contain more nanoaggregates than macroaggregates.

We also present the projections of the diffusion distribution taken on aliphatic peaks between 0 ppm and 5 ppm of the three types of asphaltenes at 15 wt % in toluene (see

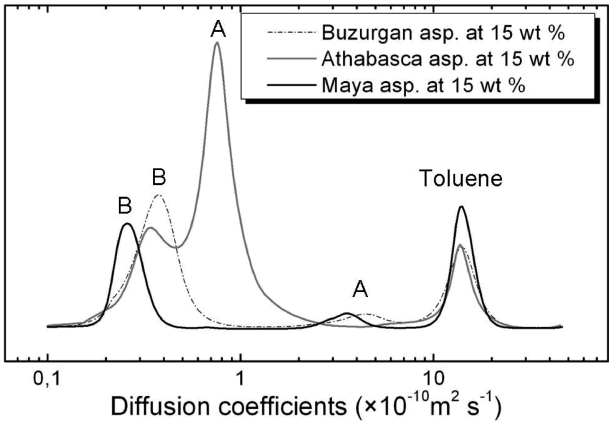


**Figure 7.** Diffusion profiles of Maya, Buzurgan, and Athabasca asphaltenes analyzed at 15 wt % in toluene-$d_8$.

**Table 3. Proportion of Nanoaggregates and Macroaggregates in Buzurgan, Maya, and Athabasca Asphaltenes at 15 wt % in Toluene-$d_8$**

| | Proportion (%) | | |
|---|---|---|---|
| aggregate | Buzurgan | Maya | Athabasca |
| nanoaggregates (peak A) | 12.0 | 14.5 | 69.3 |
| macroaggregates (peak B) | 88.0 | 85.5 | 30.7 |

Figure 7); peaks A and B are associated with nanoaggregates and macroaggregates, respectively.

Intensities correspond to arbitrary units and are not normalized. Figure 7 illustrates that the three asphaltenes fractions of different origin all show a bimodal distribution of aggregates. The asphaltene diffusion peaks are very wide, because of the polydisperse character of the asphaltenes. They are composed of thousands of molecules with a wide range of molecular weights and of chemical structures. However, the separation between the different aggregates is clearer in the case of Buzurgan and Maya asphaltenes than for the Athabasca sample. The main Athabasca peak has a double shoulder with a contribution attributed to the nanoaggregates (peak A, right-hand side) and to the macroaggregates (peak B, left-hand side). This highlights that the chemical behavior of the three investigated asphaltenes is not the same at 15 wt % in toluene-$d_8$, because the aggregation process is strongly dependent on intermolecular interactions. The relative proportion of nanoaggregates and macroaggregates of each of the asphaltene fractions analyzed at 15 wt % in toluene-$d_8$ is presented in Table 3. It shows that Athabasca asphaltenes are mainly constituted of nanoaggregates (peak A), whereas Buzurgan and Maya asphaltenes are more concentrated in macroaggregates (peak B). One can assume that the differences in nanoaggregates and macroaggregates are due to selective affinities of organic compounds for toluene. The aggregation observed by NMR occurred at a lower concentration for the Buzurgan asphaltenes than for the Athabasca asphaltenes. This is due to the fact that self-aggregation of macroaggregates (peak B) is favored in toluene. The three asphaltenes did not present the same properties in terms of mobility, number of aggregates, and isolated species.

Asphaltene behavior was investigated over a wide range of concentration (from 0.01 to 15 wt %) to highlight that the involved solute−solute and solvent−solute interactions are different. Buzurgan, Maya, and Athabasaca asphaltenes were diluted in toluene-$d_8$ and analyzed at 20 °C. The

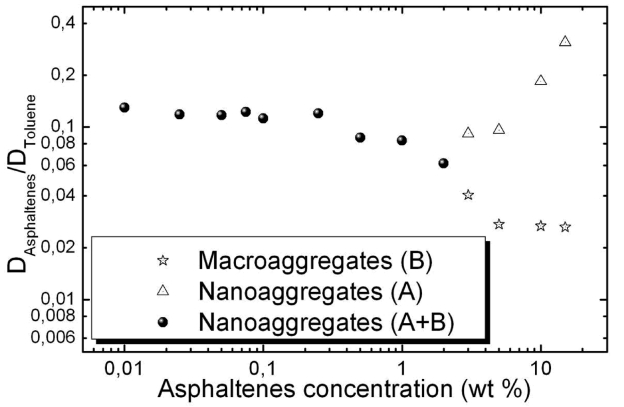


**Figure 8.** Relative diffusivities of Buzurgan asphaltenes, as a function of asphaltene concentration in toluene-$d_8$.

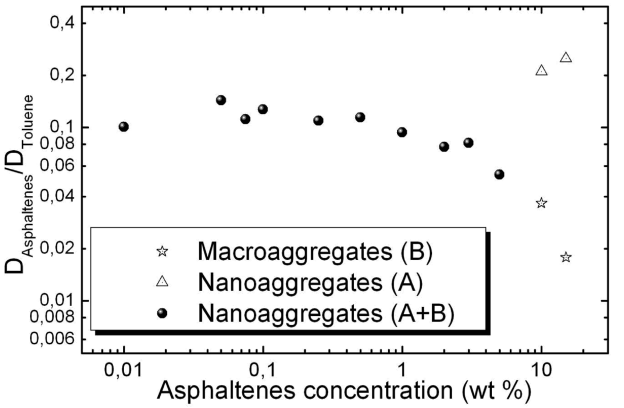


**Figure 9.** Relative diffusivities of Maya asphaltenes, as a function of asphaltene concentration in toluene-$d_8$.

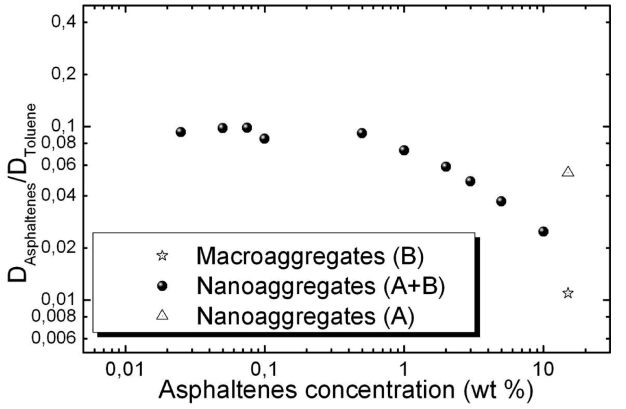


**Figure 10.** Relative diffusivities of Athabasca asphaltenes, as a function of asphaltene concentration in toluene-$d_8$.

influence of Buzurgan, Maya, and Athabasca asphaltene concentrations on their relative diffusivities ($D_{sample}/D_{solvent}$) is presented in Figures 8, 9, and 10, respectively.

The measured mobility of the solute is dependent strongly and nonlinearly upon all types of intermolecular interactions: attractive solvent−solute interactions and attractive solute−solute interactions. In fact, there is a continuous decrease in diffusion coefficient beyond 0.5 wt % for Maya and Athabasca asphaltenes and beyond 0.25 wt % for the Buzurgan asphaltenes, which is attributed to a change of regime. Below those concentrations, the solutes are isolated enough so that they are not affected by their chemical environment. In this range of concentrations, solute−solvent interactions are predominant and determine the limiting diffusion coefficient.[62] Average diffusion coefficients have been obtained on aliphatic peaks ranging from 0 ppm to 5 ppm for the asphaltenes and on aromatic peaks for toluene. Table 4 shows the solvent and solute self-diffusion and the relative diffusivity calculated for the three types of asphaltenes. Buzurgan and Maya asphaltenes show similar self-diffusion in the dilute regime, leading to similar sizes, whereas Athabasca asphaltenes diffuse more slowly. As shown in the various figures, beyond a given concentration (0.25 or 0.5 wt %, depending upon the origin of the sample), there is a semidilute regime where more-attractive interactions are involved, leading to an increase in the friction of the solute and, as a result, to a decrease in the mobility of the molecules. There are attractive solute−solute interactions, leading to an aggregation process. According to Figures 8−10, the aggregation phenomenon occurs at different concentrations. For the Buzurgan asphaltenes, both small and large aggregates were detected above 3 wt %, whereas the two aggregates were observed at 10 wt % for the Maya asphaltenes and at 15 wt % for the Athabasca sample. The presence of two different species—one diffusing quickly and one more slowly—suggests a separation of aggregates.

**Table 4. Asphaltenes and Toluene Diffusion Properties at Infinite Dilution in Toluene-$d_8$**

| | Value | | |
|---|---|---|---|
| property[a] | Buzurgan | Maya | Athabasca |
| asphaltenes self-diffusion ($\pm 0.2 \times 10^{-10}$ m$^2$/s) | 2.4 | 2.3 | 1.9 |
| toluene self-diffusion ($\pm 0.2 \times 10^{-10}$ m$^2$/s) | 19.5 | 19.5 | 19.9 |
| relative diffusivity of asphaltenes ($\pm 0.011$) | 0.121 | 0.120 | 0.094 |

[a] The values given in parentheses ($\pm x$) represent the standard deviation.

At high concentrations, the self-affinity of heavy species increases, which causes an aggregation process. Indeed, the local asphaltenes concentration in the solution varies. The aggregation of asphaltene molecules leads to a locally increase of asphaltenes concentration, and, consequently, in the neighborhood of these aggregates, less asphaltene entities are present and the remaining molecules show a higher mobility. Furthermore, the local concentration of toluene in the mixture varies: it decreases in the neighborhood of aggregated asphaltene species while the concentration of solvent increases nearby nanoaggregates, leading to an increase of the diffusion properties of these nanoaggregates.[65] Asphaltenes are known to exhibit a large polydispersity, in term of size and molecular weight.[95] As the concentration increases, the favored intermolecular interactions create a type of demixion where some molecules have a tendency to aggregate whereas small aggregates remain free in solution.[65] This behavior was established in polydispersed polymer solutions as temperature decreases, near the cloud-point transition.[96] These authors have shown, via thermodynamic calculations, that two different phases appear; the first one is enriched in high-molecular-weight polymers, while the second one mainly contains low-molecular-weight

(95) Manshad, A. K.; Edalat, M. *Energy Fuels* **2008**, *22*, 2678–2686.
(96) Behme, S.; Sadowski, G.; Arlt, W. *Fluid Phase Equilib.* **1999**, *158*, 869–877.

molecules. As a result, if some regions are becoming richer in macroaggregates of asphaltenes characterized by a low diffusion coefficient, other regions are less concentrated in macroaggregates where smaller entities remain free and can diffuse faster. Starting from a liquid mixture with a rather homogeneous distribution of asphaltenes aggregates and toluene, the increase in asphaltenes concentration is responsible for the distinction of different aggregates,[65] presenting various sizes in a macroscopic homogeneous phase. Moreover, other techniques have also confirmed some density heterogeneities in asphaltene solutions. In fact, SAXS data of Safaniya asphaltenes in toluene (6 wt %)[68] showed an upturn of the X-ray scattered intensities at very low $Q$-values (see Figures 16 and 38 in ref 68). According to the authors, this observation can be explained by density fluctuations in the medium, according to the theoretical background of the scattering techniques. Similar observations were presented by Roux et al.[97] and Sirota and Lin,[98] who mentioned a separation of phases inside the solution. More recently, Headen et al.[99] also highlighted by SANS the coexistence of big aggregates with smaller ones. However, the calculated size of the aggregates is very large (500 nm). Furthermore, Acevedo et al. have proposed to separate two fractions of asphaltenes ($A_1$ and $A_2$) using *para*-nitrophenol (PNP).[100] The fractionation basically relies on the solubility difference of these fractions (asphaltenes + PNP) in toluene. The solubility of $A_2$ is approximately equal to the entire asphaltene sample (50−100 g/L in toluene), whereas $A_1$ shows a poor solubility of 0.1 g/L.[101] According to the authors, the difference is not due to molecular weight, aromaticity, or heteroatom content, but rather is much more linked to a tridimensional structure of asphaltenes.[102] Gutierrez et al.,[100] while analyzing two fractions of asphaltenes obtained via the addition of PNP, as proposed by Acevedo et al., have concluded that asphaltenes were a mixture of compounds with different solubilities in organic solvents. According to the authors, asphaltene solutions in aromatic solvents are constituted by a colloidal phase, which has low solubility in toluene and disperses itself in a toluene-soluble fraction. Based on all this, we believe that the DOSY NMR experiments allow the detection of the beginning of an aggregation process.[65] The aggregation process is dependent on the intermolecular interactions, which can be related to the local chemical composition.

As shown above, the aggregates separation occurs at different concentrations, which illustrates that the chemical interactions (and, therefore, the chemical structure) involved are different for the three types of asphaltenes. It can also be related to a different polydispersity of the three samples. Starting from the hypothesis that asphaltenes are a mixture of both archipelago and continental asphaltenes, the interactions involved in the solutions should be different, depending on the repartition between the archipelago and continental types of asphaltenes in the medium. As reported,[103] asphaltenes of the continental type are known to self-associate by $\pi-\pi$ stacking of aromatic cores.[103] This is all the more emphasized because the toluene favors $\pi-\pi$ interactions. The most stable conformation of asphaltene aggregates with large aromatic cores showed parallel−parallel molecular stacking.[104] The steric interferences set a limit to the growth of asphaltene aggregates by stacking.[32] However, asphaltene aggregates of the archipelago type are more complex. Although ring−ring interactions are not favored, because of steric considerations, the aggregation of asphaltenes of the archipelago type occurs by bridging and hydrogen bonding.[32] Hence, asphaltenes contain some compounds that are more or less soluble in toluene. The choice of toluene enables a structural discrimination, because it acts as a good solvent for archipelago asphaltenes whereas continental asphaltenes flocculate earlier in toluene. Thus, it is obvious that aggregation between the two types of asphaltenes is not probable. In this work, when the competition between the two types of asphaltenes reaches its maximum, a separation is observed. Some dielectric constant, solubility, and flocculation experiments[105] suggested that the presence of high-polarity asphaltenes plays a key role in the stability of asphaltenes. In fact, they showed that high-polarity fractions have a great tendency to aggregate and are more difficult to remediate.[105] Continental asphaltenes are more polar than archipelago asphaltenes and are expected to aggregate more in toluene than archipelago structures. Thus, the heaviest asphaltene aggregates are thought to belong to the continental model. The self-affinity of continental asphaltenes increases with the concentration, leading to their own aggregation, characterized by a low diffusion coefficient.

We may wonder whether Buzurgan, Maya, and Athabasca asphaltenes show the same relative composition of archipelago-type asphaltenes versus continental-type asphaltenes. According to the self-diffusion of each asphaltenes in the dilute regime presented in Table 4, Maya and Buzurgan asphaltenes show similar diffusion properties in the dilute regime, whereas Athabasca asphaltenes diffuse slower than Buzurgan and Maya asphaltenes. Kuznicki et al.[103] established, using molecular dynamics simulations, that the diffusivity of the archipelago model ($(0.7 \pm 0.2) \times 10^{-10}$ m$^2$/s) was lower in toluene than the corresponding diffusivity of the continental model ($(1.2 \pm 0.8) \times 10^{-10}$ m$^2$/s). Similarly, we have shown, in previous work,[62] that, in a diesel cut, the diffusion coefficient of monoaromatics was lower than the diffusion coefficient of triaromatics, because monoaromatics in the same molecular weight range are linked to long alkyl chains. Based on the diffusion coefficients at infinite dilution (Table 4), we believe that Buzurgan asphaltenes are somewhat richer in continental-type asphaltenes than Maya asphaltenes, which are significantly more concentrated in continental-type asphaltenes than Athabasca asphaltenes. These results are in agreement with the $^{13}$C NMR data and asphaltene elemental analysis (H/C ratio). We can also look at the behavior when the two types of aggregates were observed. As mentioned above, continental-type asphaltenes are considered to self-associate more read-

(97) Roux, J. N.; Broseta, D.; Deme, B. *Langmuir* **2001**, *17*, 5085–5092.
(98) Sirota, E. B.; Lin, M. Y. *Energy Fuels* **2007**, *21*, 2809–2815.
(99) Headen, T. F.; Boek, E. S.; Stellbrink, J.; Scheven, U. M. *Langmuir* **2009**, *25*, 422–428.
(100) Gutierrez, L. B.; Ranaudo, M. A.; Mendez, B.; Acevedo, S. *Energy Fuels* **2001**, *15*, 624–628.
(101) Acevedo, S.; Cordero, T.; Carrier, H.; Bouyssiere, B.; Lobinski, R. *Energy Fuels* **2009**, *23*, 842–848.
(102) Acevedo, S.; Castro, A.; Negrin, J. G.; Fernandez, A.; Escobar, G.; Piscitelli, V.; Delolme, F.; Dessalces, G. *Energy Fuels* **2007**, *21*, 2165–2175.
(103) Kuznicki, T.; Masliyah, J. H.; Bhattacharjee, S. *Energy Fuels* **2008**, *22*, 2379–2389.
(104) Murgich, J.; Rodriguez, M. J.; Aray, Y. *Energy Fuels* **1996**, *10*, 68–76.
(105) Wattana, P.; Fogler, H. S.; Yen, A.; Garcia, M. D.; Carbognani, L. *Energy Fuels* **2005**, *19*, 101–110.

Table 5. Molecular Weight and Hydrodynamic Radius from $^1$H DOSY NMR and SEC Experiments

| property | analytical technique | Value[a] Buzurgan | Maya | Athabasca |
|---|---|---|---|---|
| $\overline{M}_n = \frac{\sum_i N_i M_i b}{\sum_i N_i}$ | SEC | 1270 (± 210) g/mol | 1070 (± 180) g/mol | 1680 (± 280) g/mol |
| | $^1$H DOSY NMR | 5890 (± 1420) g/mol | 8360 (± 2040) g/mol | 13460 (± 3590) g/mol |
| $\overline{M}_w = \frac{\sum_i N_i M_i^2 b}{\sum_i N_i M_i}$ | SEC | 4010 (± 730) g/mol | 3650 (± 670) g/mol | 6570 (± 1200) g/mol |
| | $^1$H DOSY NMR | 11170 (± 2700) g/mol | 15090 (± 3680) g/mol | 28110 (± 7500) g/mol |
| hydrodynamic radius, $R_H$ | $^1$H DOSY NMR | 15.6 (± 1.5) Å | 15.8 (± 1.6) Å | 19.6 (± 2.1) Å |

[a] The values given in parentheses (±$x$%) represent the standard deviation. [b] Based on a polystyrene equivalent.

ily than asphaltenes of the archipelago type and to form heavier asphaltene aggregates. The detected onset of flocculation was ~3 wt % for the Buzurgan asphaltenes, ~10 wt % for the Maya asphaltenes, and ~15 wt % for the Athabasca asphaltenes, which confirms the conclusion based on the diffusion coefficients at infinite dilution. Measuring the area of nanoaggregates and macroaggregates on the 2D DOSY spectrum, it was possible to estimate the relative proportion of the two types of aggregates (see Table 3). The Buzurgan asphaltenes contain 88.0% asphaltene macroaggregates, whereas the Maya asphaltenes are composed of 85.5% asphaltene macroaggregates, and the Athabasca asphaltenes show only 30.7% of this type of asphaltene aggregates. According to our previous hypothesis, we can believe that the Buzurgan asphaltenes show a more pronounced continental character than the other studied asphaltenes.

**4.3. Physical Data Extracted from the Coefficient Diffusion.** In the dilute regime (C < 0.25 wt %), the hydrodynamic radius and average molecular weight may be inferred from the mean diffusion coefficient at infinite dilution. From a macroscopic point of view, both molecular weights and hydrodynamic radius contribute to the self-diffusion coefficient. Table 4 shows the self-diffusion coefficients of Buzurgan, Maya, and Athabasca asphaltenes dissolved in toluene-$d_8$ at infinite dilutions. These values are in agreement with previous works.[66,67,71] Average hydrodynamic radii were determined (Table 5) from the self-diffusion coefficients at infinite dilution, according to the Stokes−Einstein equation (eq 3, with $f_s = 1$, average spherical particle assumed). The values obtained are in reasonable agreement with time-resolved fluorescence depolarization (TRFD),[26] fluorescence correlation spectroscopy (FCS),[66] and NMR results.[63] Based on the PS calibration curve established in previous work,[92] average molecular weights were estimated from the H-DOSY spectrum at infinite dilution of each asphaltene fraction and are presented in Table 5. Although molecular weights estimated from SAXS and SANS results are roughly a factor of 10 higher than the values presented in this study,[39,41,70] the average molecular weights presented in this article are higher than what has been recently published by several authors.[24,106] Assuming an average molecular weight in the range of 500−2000, depending on the experimental conditions, the sample, and the analytical technique used, we inferred that the average molecular weights reported in Table 5 represent the molecular weight of nanoaggregates composed of 3−55 asphaltenic molecules. One of the biggest reasons for this difference is that the experiments performed in this work are performed at concentrations much higher than those for the onset of aggregation.[20,107,108] Absorption and fluorescence spectroscopy[109] experiments showed that dimerization may occur at concentrations of 0.005 wt %, depending upon the origin of the sample. As a result, in the samples analyzed by DOSY, even at the lowest concentrations, aggregates are mixed with single molecules. Therefore, the molecular weights determined in this paper by $^1$H DOSY (polystyrene equivalent) do not represent the molecular weight of the asphaltenes monomer but that of more or less large-sized aggregates of asphaltenes.

Furthermore, the average molecular weights obtained by DOSY and SEC experiments are of the same order of magnitude, but the ranking of the asphaltenes according to molecular weight is quite different. This is not surprising, because asphaltenes were dissolved in toluene for DOSY measurements, whereas THF was used for SEC analysis. Indeed, it is proven that the nature of the solvent has a strong effect[68] on the determined molecular weights. Moreover, its effect may be dependent on whether the continental-type asphaltenes or the archipelago-type asphaltenes is more pronounced. In fact, the interactions between the solvent and the solute may differ, depending on the molecular structure. Moreover, an adsorption of compounds on the column may occur during SEC analysis, leading to underestimated apparent molecular weights. Furthermore, SEC is a technique that is based on hydrodynamic volumes of molecules and not on their mass, whereas, from a macroscopic point of view, both molecular weights and hydrodynamic radii contribute to the self-diffusion coefficients measured by $^1$H DOSY NMR.

**4.4. Structural Parameters of Asphaltene Nanoaggregates.** The data obtained by elemental analysis, $^{13}$C NMR, and DOSY NMR experiments were collected and put together to extract the average structural parameters of asphaltene nanoaggregates. Table 6 summarizes what a nanoaggregate of Buzurgan, Athabasca, and Maya asphaltenes would look like. The hydrodynamic radius ($R_H$) was deduced from the distribution of the diffusion coefficients, taking into account the highest value of the distribution and according to eq 3. The number-average molecular weight ($M_n$) and the weight-average molecular weight ($M_w$) were calculated according to the formulas given in Table 5. The parameter $I_p$ represents the polydispersity index ($M_w/M_n$). From the number-average molecular weight ($M_n$; see Table 6) and the structural parameters obtained from $^{13}$C APT NMR and elemental analysis (see Tables 1 and 2), the atomic composition of an

(106) Klein, G. C.; Kim, S.; Rodgers, R. P.; Marshall, A. G.; Yen, A. *Energy Fuels* **2006**, *20*, 1973–1979.

(107) Andersen, S. I.; del Rio, J. M.; Khvostitchenko, D.; Shakir, S.; Lira-Galeana, C. *Langmuir* **2001**, *17*, 307–313.

(108) Zeng, H.; Song, Y.-Q.; Johnson, D. L.; Mullins, O. C. *Energy Fuels* **2009**, *23*, 1201−1208.

(109) Goncalves, S.; Castillo, J.; Fernandez, A.; Hung, J. *Fuel* **2004**, *83*, 1823–1828.

**Table 6. Structural Parameters of Asphaltene Nanoaggregates**

| property | Value | | |
|---|---|---|---|
| | Buzurgan | Maya | Athabasca |
| | Physical Properties | | |
| $R$ | 15.6 ± 1.5 Å | 15.8 ± 1.6 Å | 19.6 ± 2.1 Å |
| $M_n$[a] | 5890 ± 1420 g/mol | 8360 ± 2040 g/mol | 13460 ± 3590 g/mol |
| $M_w$[a] | 11170 ± 2700 g/mol | 15090 ± 3680 g/mol | 28110 ± 7500 g/mol |
| $I_p$ | 1.9 | 1.8 | 2.1 |
| | Chemical Properties | | |
| number of carbon atoms | 399 | 581 | 900 |
| $C_{aro}$ | 212 | 322 | 452 |
| $CH_{aro}$ | 45 | 78 | 95 |
| $C_q$ | 167 | 243 | 357 |
| $C_{q,sub}$ | 91 | 119 | 185 |
| $C_{q,cond}$ | 76 | 124 | 176 |
| $C_{ali}$ | 187 | 260 | 448 |
| $C_q$ | 0 | 0 | 0 |
| CH | 26 | 48 | 63 |
| $CH_2$ | 110 | 160 | 296 |
| $CH_3$ | 49 | 52 | 94 |
| number of hydrogen atoms | 425 | 605 | 1029 |
| number of nitrogen atoms | 5 | 6 | 13 |
| number of sulfur atoms | 15 | 15 | 35 |
| number of oxygen atoms | 3 | 5 | 12 |
| maximum of rings | 35 | 53 | 75 |
| *peri*-condensed rings | 5 | 4 | 5 |
| *cata*-condensed rings | 10 | 5 | 8 |
| Predominant model | Continental | Archipelago | |

[a] Based on a polystyrene equivalent.

average asphaltene molecule having such a $M_n$ value has been reckoned. Buzurgan nanoaggregates are expected to be smaller (i.e., lower size) and lighter (i.e., lower molecular weight) than Athabasca nanoaggregates. Indeed, Athabasca nanoaggregates are composed of more atoms of carbon (and of hydrogen) than the other two samples. According to Table 6, Athabasca nanoaggregates are supposed to have a more open structure (archipelago model), composed of many long alkyl chains with much more heteroatoms (nitrogen, sulfur, and oxygen) than Buzurgan or Maya nanoaggregates. Conversely, Buzurgan and Maya nanoaggregates are expected to be more condensed with shorter chains. This table provides a molecular reconstruction of asphaltenes nanoaggregates from different origins.

## 5. Conclusions

$^1$H DOSY NMR measurements have been conducted on three asphaltenes from different origins (Buzurgan, Maya, and Athabasca asphaltenes) over a wide range of concentrations (0.01−15 wt %) in toluene-$d_8$. Results demonstrate that the asphaltenes exhibit different aggregation behaviors in toluene. In the semidilute regime, a clear separation was achieved between two classes of asphaltene aggregates: one diffusing quickly and one diffusing more slowly. We assume that asphaltene mixtures are a continuum of archipelago- and continental-type structures. The results presented seem to indicate that the interactions involved in the solutions are different, depending on the repartition between the archipelago- and continental-type asphaltenes in the medium. Furthermore, asphaltenes contain some compounds that are more or less soluble in toluene. Indeed, continental structures are more aggregated and precipitated in toluene, because $\pi-\pi$ interactions are favored in toluene.

Based on the different experimental data, Buzurgan asphaltenes seem to exhibit a more-pronounced continental character than the other studied asphaltenes, while Athabasca asphaltenes are considered to be more concentrated in archipelago-type asphaltenes. Average size and molecular weights were also determined for the three asphaltenes from the diffusion coefficients extracted from $^1$H DOSY NMR experiments and compared to SEC data.

**Acknowledgment.** The authors thank M. A. Delsuc for providing the software. They also acknowledge C. Ferreira and P. Danial Fortain for providing the SEC data.